# Effect of Sepiolite Content on Hydrophilicity and Thermal Stability of Poly(butyl lactate methacrylate)

M. Purushothaman[†,1], P. Santhana Gopala Krishnan[1,2]* and S. K. Nayak[1,2]

[1]*Department of Plastics Technology, Central Institute of Plastics Engineering and Technology, T.V.K. Industrial Estate, Guindy, Chennai-600032, India*
[2]*Department of Plastics Engineering, Central Institute of Plastics Engineering and Technology, Patia, Bhubaneswar-751024, India*
[†]*Present address: Department of Materials Engineering, Hanyang University ERICA, Ansan, Gyeonggi, 426-791, Republic of Korea*

Received September 19, 2016; Accepted February 13, 2017

**ABSTRACT:** In the present work, the hydrophilicity and thermal behavior of nanocomposites of poly(butyl lactate methacrylate) were investigated using different weight percent of sepiolite. These nanocomposites were prepared by solution casting method. X-ray diffraction (XRD) studies indicated that the increase in sepiolite content decreased the average molecular interchain spacing (<R>) values from 7.18 to 6.23 Å in nanocomposites. Apart from the amorphous halo peak of nanocomposites, the appearance of crystalline peak at 7.41° was due to the $d_{110}$ plane of sepiolite. Surface morphology of nanocomposites was studied using scanning electron microscopy (SEM) and transmission electron microscopy (TEM) techniques and the uniform dispersion of nanofiller was observed up to 1% (w/w). Depending upon the sepiolite content, relative humidity and time, the hydrophilicity of nanocomposites can be tuned to a wide range from 5.7 to 23.6% (w/w) and it follows Fickian absorption. Glass transition temperature of nanocomposites increased from 72.1 to 80.3 °C with an increase in sepiolite content. The thermal stability of nanocomposites increased with an increase in sepiolite content, which were thermally stable up to 200 °C and thereafter exhibited two-step thermal degradation in nitrogen atmosphere.

**KEYWORDS:** Nanocomposite, methacrylate, lactate, sepiolite, hydrophilicity, thermal stability

## 1 INTRODUCTION

Polymeric nanocomposites have attracted wide interest in recent years for improving the mechanical, thermal, barrier and optical properties of pristine polymers [1, 2]. Among the nanofillers, nanoclays are more attractive because of their abundance, low cost and reactivity, which make them an ideal candidate for preparing nanocomposites. Apart from these nanofillers, a natural, fibrous, phyllosilicate clay mineral of sepiolite (SP) has received much attention because of its abundance in nature, nontoxicity, high surface area and nanosized channels, which offer advantages in terms of fabricating composite with better physical, mechanical and thermal properties [3, 4]. It is a magnesium silicate that has a porous fibrous structure with internal and external channels running along the length of the fiber. The ideal half-unit cell formula of SP is $Mg_8Si_{12}O_{30}(OH)_4(H_2O)_4{\cdot}8H_2O$, where $4H_2O$ and $8H_2O$ represent coordinated and zeolitic water molecules, respectively [3, 4].

SP is used in a number of applications, including pharmaceuticals [5], filters [6], catalyst supports [7], absorbents [8], pigments [9], etc. It is also a candidate for asbestos replacement [10] because of its nontoxic nature. Because of its superior properties, SP has been used for the preparation of nanocomposites using different polymers as matrix such as poly(2-hydroxyethyl acrylate) (PHEA), acrylonitrile butadiene styrene (ABS), poly(lactic acid) (PLA), polypropylene, poly(vinyl alcohol), epoxy, polyurethane, etc. [11–16]. Volle *et al.* [11] fabricated PHEA-SP nanocomposites and evaluated the adhesion strength between the polymer matrixes and SP based on their mechanical properties. Compared to pristine polymer, the stress level reached by PHEA-SP (2.5 MPa) is higher than the stress level reached by pure PHEA (1.1 MPa). This improvement is attributed to the strong interactions at the interface between SP and PHEA. Further, Volle

*Corresponding author: psgkrishnan@hotmail.com, krishnan.psg@gmail.com

**DOI: 10.7569/JRM.2017.634128**

*et al.* [12] fabricated the nanocomposite of hydrophilic elastomers containing SP. They found that a 0.5% concentration of SP was shown to be sufficient to reinforce acrylate elastomers.

Fukushima *et al.* [13] investigated the effect of SP on the biodegradation of PLA nanocomposites. They found that PLA and PLA-SP nanocomposites seem to be mainly degraded by a bulk mechanism, showing a significant level of polymer degradation. The presence of SP particles partially delays the degradation probably due to a preventative effect of these particles on polymer chain mobility and/or PLA-enzymes miscibility. Hapuarachchi and Peijs [14] developed a fully biobased PLA composite incorporating SP nanofiller and multiwalled carbon nanotubes (MWNT). The SP nanofiller improved the flame retardancy and thermal stability of the nanocomposites along with MWNT. Acosta *et al.* [15] studied the incorporation and substitution of part of glass fiber (GF) by SP in a polypropylene composite. With 30 wt% of GF, they found an increment of 228% in flexural modulus, but in a hybrid composite with 20 wt% of GF and 10 wt% of SP, the modulus increased up to 263%. Basurto *et al.* [16] improved the stiffness, Young's modulus and HDT of ABS nanocomposites by the reinforcement of GF and SP. But they observed that the decrease in matrix toughness was associated with the stress-zones generated by GF and SP.

In our previous work, we synthesized a series of poly(alkyl lactate acrylate)s [17, 18], poly(alkyl lactate methacrylate)s [19] and copolymers with acrylic acid [20, 21]. Among the homopolymers, poly(butyl lactate methacrylate) (PBLM) exhibited highest moisture absorption of about 24% (w/w) at 97% relative humidity (RH) in 30 ± 1 °C. In our present work, we incorporated SP nanofiller in PBLM to further enhance the properties. The main objective of this work is to modify the hydrophilicity and thermal stability of PBLM using SP nanofiller which is a good absorbent for aqueous and organic compounds. It has active absorption sites, highest surface area (150–320 $m^2/g$), and crystal defects, which increase its absorption behavior for wide use in the fields of percolation absorbents, floor absorbents, oil refining, wastewater treatment, odor removal, pesticide carriers, drilling fluids, paints, paper, washing powders, etc. [3]. Because of its superior properties, SP has been used for the preparation of nanocomposites with PBLM polymer matrix. In a continuation of the previous work, nanocomposites of PBLM were synthesized with different weight percentage of SP content to tune the properties of nanocomposites such as average molecular interchain spacing (<R>), hydrophilicity, glass transition temperature ($T_g$) and thermal stability.

## 2 EXPERIMENTAL

### 2.1 Materials

Free-radical solution polymerization technique was used to synthesize PBLM in a similar procedure reported elsewhere [21]. SP nanofiller (thickness: 5–15 nm; width: 10–30 nm; length: 500–5000 nm in size) was purchased from Sigma-Aldrich chemicals. All other chemicals were used as received.

### 2.2 Synthesis of Polymer Nanocomposites

Poly(butyl lactate methacrylate) was used to prepare polymer nanocomposites by solution casting method using SP nanofiller of 0.5, 1.0, 1.5 and 2.0% (w/w) with respect to polymer content. Initially, PBLM (0.995 g) was dissolved in tetrahydrofuran (25 mL), followed by the gradual addition of SP (0.005 g) using a magnetic stirrer at 1000 rpm. Later, the solution was sonicated for about 30 min at room temperature using an ultrasonicator. The frequency and amplitude used for dispersion of SP were 33 ± 3 kHz and 100%, respectively. The resulting mixture was solution casted on a clean glass plate and kept in a vacuum oven at 40 °C for 12 hours to get 0.5% (w/w) nanocomposite [22]. Similarly, other nanocomposites were prepared for the remaining concentration of SP nanofiller and the sample codes are given in Table 1.

### 2.3 Characterization

A Thermo Scientific Nicolet 6700 spectrometer was used to record the Fourier transform infrared (FTIR) spectra in the range of 4000 to 400 $cm^{-1}$. X-ray diffraction (XRD) measurements were carried out using a Shimadzu Lab XRD-6000 instrument with $CuK_\alpha$ radiation (40kV, 30mA) having a wavelength of 1.54 Å. Morphologies of nanocomposites were studied using scanning electron microscopy (SEM) and transmission electron microscopy (TEM). SEM micrographs were obtained with the help of a Carl Ziess SMT (EVO MA15) scanning electron microscope. The nanocomposite samples were conditioned for 1 h and sputter coated with gold before imaging using an accelerating voltage of 5–20 kV. The TEM images were recorded using a JEM 1400 (JEOL, Japan) instrument with an acceleration voltage of 100 kV. The samples were trimmed by ultramicrotome using a diamond knife to about 70 nm thickness and ultrathin sections were placed on 300-mesh carbon-coated copper grids for observations. Moisture absorption at 30 ± 1 °C was measured gravimetrically in 69, 86 and 97% RH using a digital weighing balance. A PerkinElmer DSC Diamond Differential Scanning Calorimeter was

used to measure thermal transitions at a heating rate of 10 °C/min using 4–6 mg of sample in an aluminum pan. Weight loss was examined using a PerkinElmer Pyris1 TGA at a heating rate of 10 °C/min in $N_2$ atmosphere with a sample weight of 4–6 mg.

## 3 RESULTS AND DISCUSSION

### 3.1 FTIR Spectroscopy

The typical FTIR spectra of SP, PBLM and 1.0-PBLM are shown in Figure 1. The FTIR spectrum of SP [23] exhibited Si-O stretching vibration peaks at 1011.8, 977.8 $cm^{-1}$ and bending vibration peak at 460.0 $cm^{-1}$ (Figure 1). The observed stretching peak at 439.6 $cm^{-1}$ was due to the presence of Si-O-Mg [23]. Apart from the PBLM peaks, the FTIR spectrum of 1.0-PBLM indicated the appearance of Si-O and Si-O-Mg peaks at 457.3 $cm^{-1}$ and 437.5 $cm^{-1}$ and confirmed the incorporation of SP into PBLM matrix. In the FTIR spectrum of 1.0-PBLM (Figure 1), the characteristic IR peaks of C-H, C=O, Si-O and Si-O-Mg were observed to lower wave number value compared to PBLM and SP. These shifts in wave number value indicated that the interaction between polymer and nanofiller is strong.

### 3.2 XRD Analysis of Nanocomposites

Figure 2 represents the typical XRD pattern of SP and 1.0-PBLM nanocomposites. The appearance of peak at 7.41° in XRD with 100% relative intensity was due to the $d_{110}$ plane of SP. Apart from the peak at 7.41° ($d_{110}$) of SP, it also exhibited sharp 2$\theta$ peaks at 19.75 ($d_{060}$), 20.65 ($d_{131}$), 26.79 ($d_{400}$), 35.02 ($d_{191}$) and many small peaks [24, 25]. The absence of 2$\theta$ peaks at 30.88° and 41.04° confirmed that the SP nanofiller was free from dolomite impurities [26]. The synthesized PBLM-SP nanocomposites were amorphous, as indicated by a broad amorphous halo peak (Figure 2). Increase in the SP content in polymer matrix increases the 2$\theta$ values of amorphous halo from 15.39 to 17.79°, which is due to the strong interaction between the PBLM and SP nanofiller. The appearance of 2$\theta$ peak at about 7.4° in PBLM nanocomposites confirmed the incorporation of SP into polymer matrix.

The d-spacing of 110 plane of SP in nanocomposite samples was calculated using Bragg's Equation:

$$n\lambda = 2d\sin\theta \qquad \text{or} \qquad d = \frac{n\lambda}{2\sin\theta} \qquad (1)$$

where $d$ is the interplanar spacing of SP at $d_{110}$ plane, $\lambda$ is the wavelength of radiation (Cu $K_\alpha$, $\lambda$ = 1.5418 Å), $\theta$ is diffraction maximum angle obtained from $d_{110}$ plane and $n$ = 1. The calculated d-spacing value of $d_{110}$ plane of SP and PBLM-SP nanocomposites are given in Table 1. The calculated d-spacing value of SP is 1.19 nm ($d_{110}$). A similar observation was made by Shafiq *et al.* [23] and their reported d-spacing value was 1.22 nm ($d_{110}$), which was comparable with studied SP nanofiller. The d-spacing value of 110 plane of SP was increased from 1.19 to 1.28 nm with an increase in the SP content in PBLM, which is due to the strong intercalation of SP nanofiller with polymer matrix. The nanocomposites did not exhibit other crystalline peaks of SP, which were overlapped with polymer amorphous halo.

For amorphous materials, the average molecular interchain spacing (<R>) and spacing between adjacent parallel polymer chains were calculated using

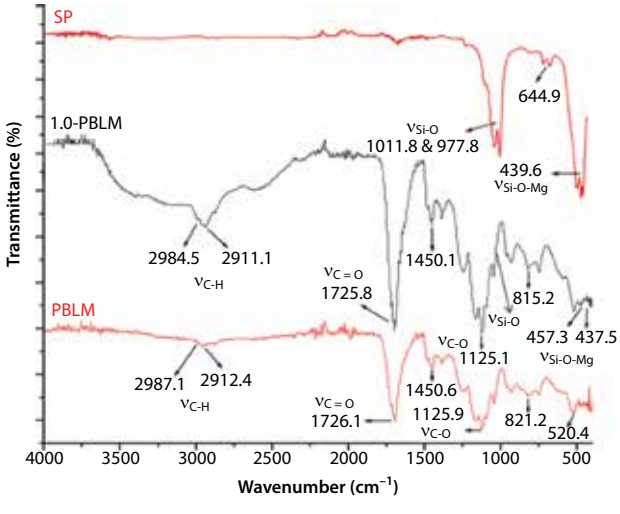


**Figure 1** FTIR spectra of (**a**) SP, (**b**) 1.0-PBLM and (**c**) PBLM.

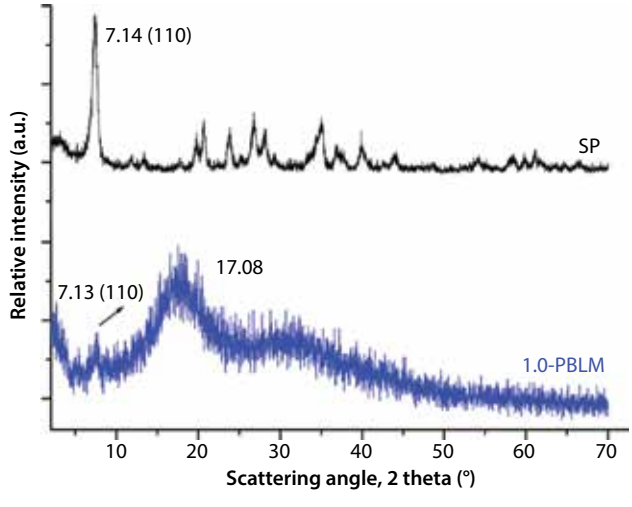


**Figure 2** XRD pattern of (**a**) SP and (**b**) 1.0-PBLM.

**Table 1** Sample code and XRD data of PBLM-SP nanocomposites.

| Material | Sepiolite (%, w/w) | Sample code | XRD data | | | |
|---|---|---|---|---|---|---|
| | | | 2θ (°) (Amorphous Halo) | <R> (Å) | 2θ (°) (SP (110) plane) | d (nm) |
| Sepiolite | – | SP | – | – | 7.41 | 1.19 |
| PBLM | 0 | PBLM | 15.39 | 7.18 | – | – |
| | 0.5 | 0.5-PBLM | 16.79 | 6.60 | 7.42 | 1.19 |
| | 1.0 | 1.0-PBLM | 17.08 | 6.49 | 7.13 | 1.24 |
| | 1.5 | 1.5-PBLM | 17.68 | 6.27 | 7.01 | 1.26 |
| | 2.0 | 2.0-PBLM | 17.79 | 6.23 | 6.88 | 1.28 |

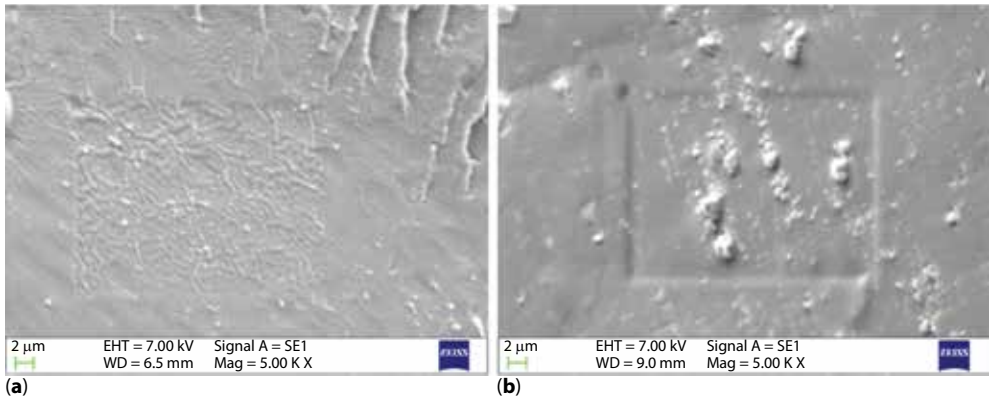

(**a**) (**b**)

**Figure 3** SEM microimages of (**a**) 1.0-PBLM and (**b**) 1.5-PBLM.

Equation 2 [27] and the calculated <R> values are given in Table 1.

$$< R >= \frac{5}{8}\left[\frac{\lambda}{\sin\theta}\right] \quad (2)$$

where $\lambda$ is the wavelength of radiation and $\theta$ is diffraction maximum angle. The <R> values of nanocomposites decreased with the increase in the SP content from 0.5 to 2.0% (w/w). The incorporation of SP in polymer matrix decreased the <R> value which is indicative of the fact that the free volume decreased after the introduction of SP.

## 3.3 SEM Analysis

To analyze the extent of dispersion of nanofiller into polymer matrix a morphological investigation of the nanocomposite surface was conducted using SEM. Figure 3 represents the typical SEM micrographs of 1.0-PBLM and 1.5-PBLM nanocomposites. The micrographs of nanocomposites revealed that the dispersion of SP was uniform at 1% (w/w) (Figure 3a) and the dispersion was not uniform and agglomeration had taken place at 1.5% concentration (Figure 3b).

## 3.4 TEM Analysis

Figure 4 shows typical TEM images of SP, 1.0-PBLM and 1.5-PBLM. The TEM image in Figure 4a confirms the fiber structure of SP. The incorporation of SP up to 1% (w/w) into polymer matrix of PBLM exhibited uniform dispersion (Figure 4b); thereafter agglomeration was observed at higher loading of SP (Figure 4c).

## 3.5 Hydrophilicity

The effect of SP content from 0.5 to 2.0% (w/w) on the moisture absorption ability of PBLM matrix was investigated in different RHs such as 69, 86 and 97%. The moisture absorption percentage was calculated from the weight gain with respect to dried sample weight. The moisture absorption of copolymers as a function of time plotted at 69, 86 and 97% RH is shown in Figures 5, 6 and 7 respectively. In all these

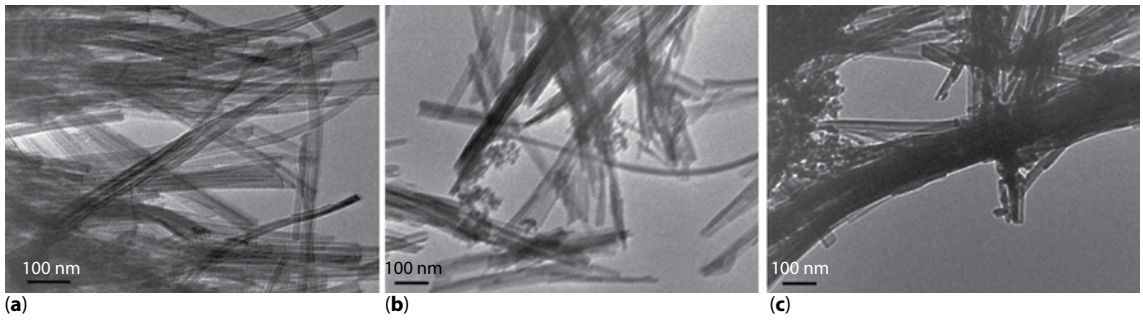


**Figure 4** TEM images of (**a**) SP, (**b**) 1.0-PBLM and (**c**) 1.5-PBLM.

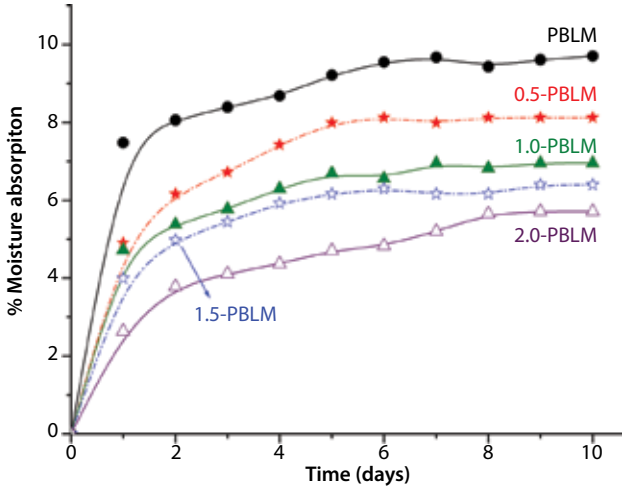


**Figure 5** Plot of % moisture absorption vs. time of PBLM-SP nanocomposites at 69% RH.

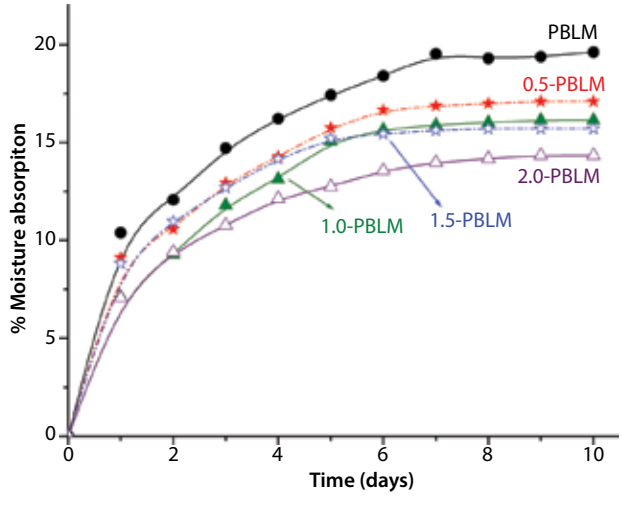


**Figure 6** Plot of % moisture absorption vs. time of PBLM-SP nanocomposites at 86% RH.

cases, moisture absorption values decreased with the increase in SP content.

Equilibrium moisture absorption ($M_e$) was calculated from the above moisture absorption data. The

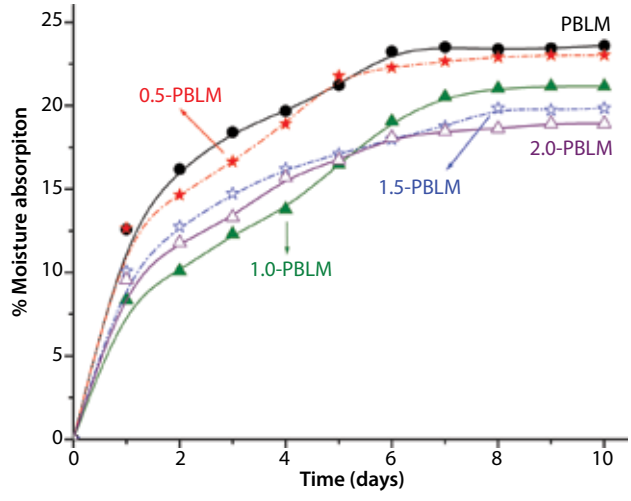


**Figure 7** Plot of % moisture absorption vs. time of PBLM-SP nanocomposites at 97% RH.

$M_e$ shows that the moisture absorption of PBLM-SP nanocomposites are neither gaining nor losing moisture; however, this is a dynamic equilibrium and changes with relative humidity, time and temperature. The $M_e$ value of nanocomposites decreased from 9.7 to 5.7% (w/w) at 69% RH, 19.6 to 14.3% (w/w) at 86% RH and 23.6 to 18.9% (w/w) at 97% RH depending upon the content of SP in PBLM matrix. The $M_e$ values of nanocomposites are given in Table 2. Reduction in $M_e$ values was attributed to the reduction in <R> value (Table 2). Lower <R> value indicated that the free volume has come down. Using the SP nanofiller, one can tune the hydrophilicity of polymer with respect to different weight loadings.

Figure 8 represents the plot of SP content vs. $M_e$ of PBLM-SP nanocomposites. From this plot, one can predict the $M_e$ value at specified RH for the different weight percentage of SP content up to 2% (w/w). Depending upon the application requirements, hydrophilicity can be tuned with respect to nanofiller loading.

 DOI: 10.7569/JRM.2017.634128

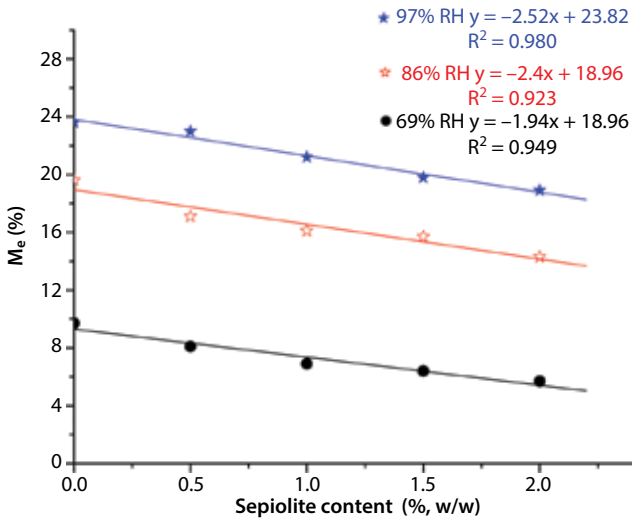


**Figure 8** Plot of $M_e$ vs. SP content of PBLM-SP nanocomposites.

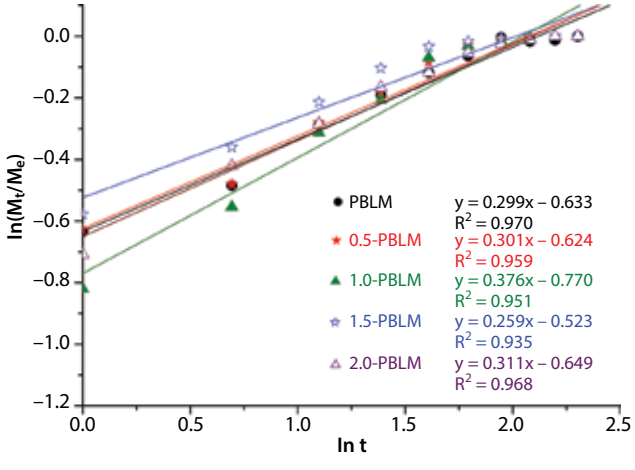


**Figure 9** Plot of $\ln(M_t/M_e)$ vs. $\ln t$ for the moisture absorption of PBLM-SP nanocomposites at 86% RH.

The hydrophilicity data was analyzed using the following equation in order to know the type of absorption process:

$$\frac{M_t}{M_e} = kt^n \tag{3}$$

where $M_t$ is the amount of moisture absorption at time $t$ and $M_e$ is the equilibrium moisture absorption, $k$ is the characteristic constant of polymer and $n$ is a characteristic exponent of the mode of transport of the penetrating molecule [28]. It is noted that for a Fickian process the value of $n$ is less than 0.5, whereas the value of $n$ between 0.5 and 1.0 indicates a non-Fickian process. The plot of $\ln (M_t/M_e)$ against $\ln t$ at 86% RH is given in Figure 9. The obtained values are tabulated in Table 2. The $n$ value of nanocomposites below 0.5 indicated that the nanocomposites followed Fickian absorption.

## 3.6 DSC Analysis

Figure 10 represents the DSC curves of PBLM-SP nanocomposites. The $T_g$ values of nanocomposites increased with an increase in SP content from 72.1 to 80.3 °C, which was attributed to the reduction in the free volume. A decrease in the <R> value of nanocomposites (Table 1) was also indicative of a decrease in free volume. A similar trend was reported for PLA nanocomposites containing SP nanofiller [13, 14].

## 3.7 TGA Studies

Thermograms of PBLM-SP nancomposites are given in Figure 11. Thermal stability of the nanocomposites in nitrogen atmosphere was assessed by comparing 10, 25, 50 and 75% weight loss and $T_{max}$ values

**Table 2** $M_e$, $n$ and $k$ parameters for moisture absorption of PBLM-SP nanocomposites.

| | $M_e$ (%) | | | $n$ | | | k | | |
|---|---|---|---|---|---|---|---|---|---|
| **Nanocomposite** | **69% RH** | **86% RH** | **97% RH** | **69% RH** | **86% RH** | **97% RH** | **69% RH** | **86% RH** | **97% RH** |
| PBLM | 9.7 | 19.6 | 23.6 | 0.12 | 0.29 | 0.28 | 0.77 | 0.53 | 0.56 |
| 0.5-PBLM | 8.1 | 17.1 | 23.0 | 0.22 | 0.30 | 0.29 | 0.64 | 0.54 | 0.54 |
| 1-PBLM | 6.9 | 16.1 | 21.2 | 0.18 | 0.38 | 0.46 | 0.69 | 0.46 | 0.37 |
| 1.5-PBLM | 6.4 | 15.7 | 19.8 | 0.19 | 0.26 | 0.30 | 0.67 | 0.59 | 0.52 |
| 2-PBLM | 5.7 | 14.3 | 18.9 | 0.32 | 0.31 | 0.32 | 0.49 | 0.52 | 0.49 |

 

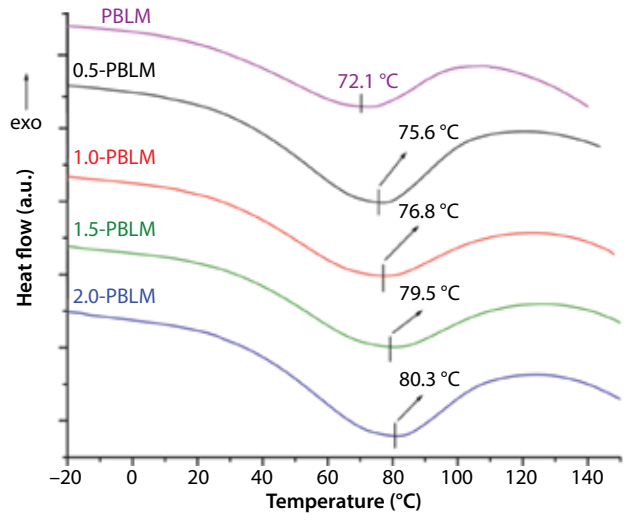


**Figure 10** DSC curves of PBLM-SP nanocomposites.

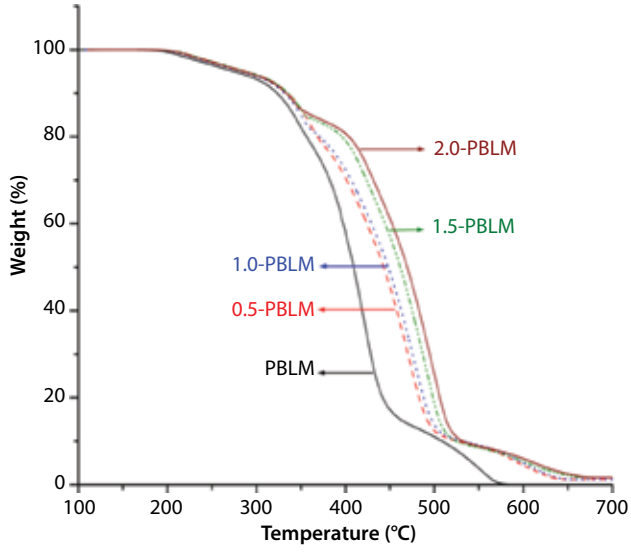


**Figure 11** Thermogram of PBLM-SP nanocomposites.

(Table 3). All the nanocomposite samples showed prominent two-step thermal degradation. The first step of the degradation is due to the breakdown of butyl lactate pendant group and loss of water molecules present in the SP nanofiller. The second step is due to the random chain scission of polymer backbone. Comparing the thermal stability and $T_{max}$ values of PBLM with PBLM nanocomposites (Table 3), all of the nanocomposites exhibited higher thermal stability than PBLM. This is due to the interaction between the polar groups of SP and PBLM matrix, which increased the thermal stability. From the XRD results, it is also concluded that intercalation of SP nanofiller increased the surface area of SP in the polymer matrix, which increased the interaction of SP with PBLM, resulting in the enhanced thermal stability of nanocomposites. A similar trend was observed for $T_{max}$ values of nanocomposites. The $T_{max}$ values indicated the substantial increase in thermal stability of nanocomposites upon incorporation of SP nanofiller. The residue percentage increased with an increase in the nanofiller content.

## 4 CONCLUSIONS

Nanocomposites of PBLM were successfully prepared by varying the SP content from 0.5 to 2.0% (w/w) by solution casting method. A shift in the peak values of FTIR and XRD indicates that SP nanofiller had a strong interaction with PBLM matrix. SEM and TEM micrographs confirmed the uniform distribution of SP up to 1% (w/w). Hydrophilicity of nanocomposites followed Fickian absorption and can be tuned to a wide range from 5.7 to 23.6% (w/w) depending upon the application requirement. The $T_g$ and thermal stability of nanocomposites increased with an increase in SP content, but decreased <R> value. A correlation existed between <R>, hydrophilicity and $T_g$.

**Table 3** TGA data of PBLM-SP nanocomposites.

| Nanocomposite | % wt loss (°C) | | | | $T_{max}$ (°C) | Residue at 700 °C (%) |
|---|---|---|---|---|---|---|
| | 10% | 25% | 50% | 75% | | |
| PBLM | 323 | 371 | 409 | 434 | 424 | 0 |
| 0.5-PBLM | 331 | 387 | 440 | 469 | 473 | 1.2 |
| 1.0-PBLM | 334 | 392 | 448 | 482 | 479 | 1.4 |
| 1.5-PBLM | 335 | 413 | 462 | 493 | 492 | 2.1 |
| 2.0-PBLM | 336 | 420 | 469 | 501 | 501 | 2.4 |

## ACKNOWLEDGMENT

Financial support given by Central Institute of Plastics Engineering and Technology under Center of Excellence for Green Transportation Network (CoE-GREET) sponsored by the Department of Chemicals and Petrochemicals, Ministry of Chemicals and Fertilizers, Government of India, is gratefully acknowledged.

## REFERENCES

1. K. Fukushima, D. Tabuani, and G. Camino, Nanocomposites of PLA and PCL based on montmorillonite and sepiolite. *Mater. Sci. Eng. C* **29**, 1433–1441 (2009).
2. S.S. Ray and M. Okamoto, Polymer/layered silicate nanocomposites: A review from preparation to processing. *Prog. Poly. Sci.* **28**, 1539–1641 (2003).
3. M. Alkan, G. Tekin, and H. Namli, FTIR and zeta potential measurements of sepiolite treated with some organosilanes. *Micropor. Mesopor. Mater.* **84**, 75–83 (2005).
4. M. Rautureau and C. Tchoubar, Structural analysis of sepiolite by selected area electron diffraction-relations with physico-chemical properties. *Clays Clay Miner.* **24**, 43–49 (1976).
5. M. Sugiura, M. Horii, H. Hayashi, and M. Sasayama, Application of sepiolite to prevent bleeding and blooming for EPDM rubber composition. *Appl. Clay Sci.* **11**, 89–97 (1996).
6. M.R. Weir, E. Rutinduka, C. Detellier, C.Y. Feng, Q. Wang, T. Matsuura, and R. Le-van-mao, Fabrication, characterization and preliminary testing of all-inorganic ultrafiltration membranes composed entirely of a naturally occurring sepiolite clay mineral. *J. Membr. Sci.* **182**, 41–50 (2001).
7. A.J. Aznar, E. Gutierrez, P. Diaz, A. Alvarez, and G. Poncelet, Silica from sepiolite: Preparation, textural properties, and use as support to catalysts. *Micropor. Mat.* **6**, 105–114 (1996).
8. A. Rodriguez, G. Ovejero, M. Mestanza, and J. Garcia, Removal of dyes from wastewaters by adsorption on sepiolite and pansil. *Ind. Eng. Chem. Res.* **49**, 3207–3216 (2010).
9. R. Giustetto, O. Wahyudi, I. Corazzari, and F. Turci, Chemical stability and dehydration behavior of a sepiolite/indigo Maya Blue pigment. *Appl. Clay. Sci.* **52**, 41–50 (2011).
10. H. Noda, K. Miyagawa, M. Kobayashi, H. Horiguchi, K. Ozawa, N. Kumada, Y. Yonesaki, T. Takei, and N. Kinomura, Preparation of cordierite from fibrous sepiolite. *J. Ceram. Soc. Jpn.* **117**, 1236–1239 (2009).
11. N. Volle, A. Burr, F. Giulieri, S. Pagnotta, and A.M. Chaze, Maya Blue as natural coloring fillers in a multi-scale polymer-clay nanocomposite. *Compos. Sci. Technol.* **71**, 1685–1691 (2011).
12. N. Volle, F. Giulieri, A. Burr, S. Pagnotta, and A.M. Chaze, Controlled interactions between silanol groups at the surface of sepiolite and an acrylate matrix: Consequences on the thermal and mechanical properties. *Mater. Chem. Phys.* **134**, 417–424 (2012).
13. K. Fukushima, D. Tabuani, and G. Camino, Nanocomposites of PLA and PCL based on montmorillonite and sepiolite. *Mater. Sci. Eng. C* **29**, 1433–1441 (2009).
14. T.D. Hapuarachchin and T. Peijs, Multiwalled carbon nanotubes and sepiolite nanoclays as flame retardants for polylactide and its natural fibre reinforced composites. *Compos. A* **41**, 954–963 (2010).
15. J.L. Acosta, E. Morales, M.C. Ojeda, and A. Linares, Effect of addition of sepiolite on the mechanical properties of glass fiber reinforced polypropylene. *Angew. Makromol. Chem.* **138**, 103–110 (1986).
16. F.C. Basurto, D. Garcia-Lopez, N. Villarreal-Bastardo, J.C. Merino, and J.M. Pastor, Composites and nanocomposites of ABS: Synergy between glass fiber and nanosepiolite. *Compos. B Eng.* **47**, 42–47 (2013).
17. M. Purushothaman, P.S.G. Krishnan, and S.K. Nayak, Poly(alkyl lactate acrylate)s having tunable hydrophilicity. *J. Appl. Polym. Sci.* DOI: 10.1002/APP.40962 (2014).
18. M. Purushothaman, P.S.G. Krishnan, and S.K. Nayak, Effect of isoalkyl lactates as pendant group on poly(acrylic acid). *J. Macromol. Sci. A Pure. Appl. Chem.* **51**, 470–480 (2014).
19. M. Purushothaman, P.S.G. Krishnan, and S.K. Nayak, Studies on hydrophilicity and thermal stability of poly(isoalkyl lactate methacrylate)s. *J. Macromol. Sci. A Pure. Appl. Chem.* **52**, 202–209 (2015).
20. M. Purushothaman, P.S.G. Krishnan, and S.K. Nayak, Tunable hydrophilicity of poly(ethyl lactate acrylate-co-acrylic acid). *J. Renew. Mater.* **3**, 292–301 (2015).
21. M. Purushothaman, P.S.G. Krishnan, and S.K. Nayak, Effect of butyl lactate methacrylate content on the properties of acrylic acid copolymers. *Polym. Sci. A* **58**, 368–378 (2016).
22. P.S.G. Krishnan, A.E. Wisanto, S. Osiyemi, and C. Ling, Synthesis and properties of BCDA-based polyimide-clay nanocomposites. *Polym. Int.* **56**, 787–795 (2007).
23. M. Shafiq, T. Yasin, and S. Saeed, Synthesis and characterization of linear low-density polyethylene/sepiolite nanocomposites. *J. Appl. Polym. Sci.* **123**, 1718–1723 (2012).
24. A.L. Vicosa, A.C.O. Gomes, B.G. Soares, and C.M. Paranhos, Effect of sepiolite on the physical properties and swelling behavior of rifampicin-loaded nanocomposite hydrogel. *Express Polym. Lett.* **3**, 518–524 (2009).
25. V. Peinado, L. Garcia, A. Fernandez, and P. Castell, Novel lightweight foamed poly(lactic acid) reinforced with different loadings of functionalised sepiolite. *Compos. Sci. Technol.* **110**, 17–23 (2014).
26. A. Tabak, E. Eren, B. Afsin, and B. Caglar, Determination of adsorptive properties of a Turkish sepiolite for removal of reactive blue 15 anionic dye from aqueous solutions. *J. Hazard. Mater.* **161**, 1087–1094 (2009).
27. A.F. Halasa, G.D. Wathen, W.L. Hsu, B.A. Matrana, and J.M. Massie, Relationship between interchain spacing of amorphous polymers and blend miscibility as determined by wide-angle X-ray scattering. *J. Appl. Polym. Sci.* **43**, 183–190 (1991).
28. N.M. Franson and N.A. Peppas, Influence of copolymer composition on non-fickian water transport through glassy copolymers. *J. Appl. Polym. Sci.* **28**, 1299–1310 (1983).